Advances in Molten Slags, Fluxes, and Salts: Proceedings of The 10th International Conference on Molten Slags, Fluxes and Salts (MOLTEN16)
Edited by: Ramana G. Reddy, Pinakin Chaubal, P. Chris Pistorius, and Uday Pal
TMS (The Minerals, Metals & Materials Society), 2016

REVIEW OF LIQUIDUS SURFACE AND PHASE EQUILIBRIA IN THE TiO_2-SiO_2-Al_2O_3-MgO-CaO SLAG SYSTEM AT PO_2 APPLICABLE IN FLUXED TITANIFEROUS MAGNETITE SMELTING

[1,3]**Xolisa Goso,** [2]**Johannes Nell,** [3]**Jochen Petersen**

[1]Mintek, 200 Malibongwe Drive, Private Bag X3015, Randburg, 2125, South Africa
XolisaG@mintek.co.za
[2]Hatch, Private Bag X20, Gallo Manor, 2052, South Africa
[3]University of Cape Town, Private Bag X3, Chemical Engineering Building, Rondebosch, 7701, South Africa

Keywords: Titanomagnetite slag, liquidus surface, phase equilibria, FactSage

Abstract

The current liquidus surface and phase equilibria established in air for fluxed titaniferous magnetite (titanomagnetite) slags conforming to a composition of 37.19% TiO_2, 19.69% SiO_2, 13.12% Al_2O_3, and 30.00% of various ratios of CaO+MgO were reviewed at applicable PO_2 using FactSage simulation and phase composition of a real plant titanomagnetite slag. The testwork included the incorporation into FactSage of a private $MgTi_2O_5$-Al_2TiO_5 pseudobrookite solution model. The results of the investigation showed that the liquidus surface and Ti^{3+}/ Ti^{4+} mass fraction ratio increased with decreasing the PO_2. At low PO_2, perovskite crystallizes as a primary phase at high CaO content. The spinel solution, i.e. $(Mg)(Al,Ti)O_4$, generally crystallizes as the primary phase at high MgO contents, though it is replaced by $MgTi_2O_5$-Al_2TiO_5 solution at PO_2 of 10^{-10} atm to 10^{-15} atm. An intermediate equilibrium phase diagram established at PO_2 of 10^{-16} atm is proposed. This phase diagram does not show the observed primary phase crystallization competition, however, the phase composition of a real titanomagnetite slag produced by Evraz Highveld Steel and Vanadium Corporation in South Africa does show primary phase crystallization competition between $(Mg)(Al,Ti)_2O_4$ and $MgTi_2O_5$-Al_2TiO_5. Smelting involving such slags is likely conducted around the transition PO_2, i.e. PO_2 of about 10^{-16} atm. Complex modelling with $MgTi_2O_5$, Al_2TiO_5 and Ti_3O_5 end members and experiments are underway to verify and update the intermediate phase diagram.

Introduction

Titanomagnetite is typically smelted in the presence of fluxes such as silica, dolomite and/or limestone, to produce a valuable high vanadium pig iron metal and a valueless TiO_2 (titania) bearing slag. The titanomagnetite slags conform to the TiO_2-SiO_2-Al_2O_3-MgO-CaO system and contain between 20 and 40% TiO_2 [1-3]. Several complex processes have been proposed for processing low-titania resources, including titanomagnetite slags, to marketable titania materials [4-7]. To date, these processes have not been implemented because they are not economically viable and produce insufficient TiO_2 grades to qualify as titania products [8]. A titanomagnetite slag with the right chemistry for subsequent TiO_2 recovery is desired.

Zhao et al [9] reviewed phase equilibria in the TiO_2-SiO_2-Al_2O_3-MgO-CaO system applicable to blast furnace ironmaking slag, i.e. <10% TiO_2, at carbon saturation, and found crystallization of

reduced titanium species (Ti^{3+}) in the pseudobrookite primary phase. Jochens et al [10] established an equilibrium phase diagram in an air atmosphere (referred to henceforth as "current phase diagram") for titanomagnetite slags that conform to a composition: 19.69% SiO_2, 13.12% Al_2O_3, 37.19% TiO_2 and 30.00% of various ratios of CaO+MgO. This is shown in Figure 1. The composition is typical of a slag produced from dolomite-fluxed smelting of South Africa's Bushveld Complex titanomagnetite. The primary phases in the phase diagram are perovskite ($CaTiO_3$) and a pseudobrookite solid solution ($MgTi_2O_5$-Al_2TiO_5) at high CaO and MgO, respectively [10]. As a consequence of the current phase diagram having been established in air, the presence of reduced titanium species such as Ti^{3+} reported by Zhao et al [9] are not included in the work of Jochens et al [10]. This is relevant since titanomagnetite slag is produced under very reducing conditions rather than in air.

The focus of the current study was thus to use FactSage thermochemical modelling software[11] to review the equilibrium phase diagram, produced by Jochens et al [10], at a range of PO_2 applicable to fluxed reductive smelting of titanomagnetite. This involved thermodynamic modeling for the development of a private $MgTi_2O_5$-Al_2TiO_5 solid solution database on FactSage, as well as the employment of the FactSage software to build on the work of Jochens et al [10] by implementing applicable PO_2 in the same slag compositions. The scope of work also included the examination of a real plant titanomagnetite slag composition.

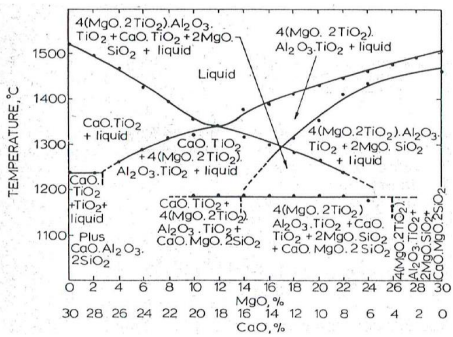

Figure 1: Equilibrium phase diagram in air for the slag system: TiO_2 = 37.19%, SiO_2 = 19.69%, and Al_2O_3 = 13.12, at varying proportions of CaO (30-%0) and MgO (0-30%)

Thermodynamic modelling

The latest version of FactSage (7.0) used in the current work contains data for all the essential compounds, including pseudobrookite-type compounds such as karrooite ($MgTi_2O_5$) and tialite (Al_2TiO_5). However, Al_2TiO_5 was not modelled as a component in the custom pseudobrookite solution. A private pseudobrookite solution database for $MgTi_2O_5$-Al_2TiO_5 therefore needed to be developed and subsequently incorporated into FactSage. In this first stage of the multi-stage study, although it is expected to be an important endmember under reducing conditions, Ti_3O_5 was not modelled as a component of the private $MgTi_2O_5$-Al_2TiO_5 solution.

In the development of the private $MgTi_2O_5$-Al_2TiO_5 solid solution database, regular or non-ideal mixing of the respective pseudobrookite-type compounds was adopted to describe the thermodynamic properties of the solid solution [12]. The $MgTi_2O_5$-Al_2TiO_5 solid solution is considered to be composed of cationic sublattices A and B, and an anionic (O^{2-}) sublattice C. A random distribution of Mg^{2+}, Ti^{4+} and Al^{3+} in the cationic sublattices at high temperatures is assumed [12- 15]. The current modelling of $MgTi_2O_5$-Al_2TiO_5 followed a successful approach implemented by previous researchers in modelling related pseudobrookite-type solutions [16, 17]. The same model is adopted in which the $MgTi_2O_5$-Al_2TiO_5 solution is taken as $\left(Mg^{2+}_{1-x}Al^{3+}_{x}\right)_A\left(Ti^{4+}_{2-x}Al^{3+}_{x}\right)_B O_5$. $(1-x)$ and x represent the overall mole fractions of $MgTi_2O_5$ and Al_2TiO_5, respectively. The $MgTi_2O_5$-Al_2TiO_5 solution is assumed to consist of four endmembers, namely: the real component $MgTi_2O_5$, and three pseudocomponents $Al_3O_5^-$, $AlTi_2O_5^+$, and $MgAl_2O_5^{2-}$. The molar Gibbs energy of the solution is given by the following expression [16, 17]:

$$G = (1-x)\left(\frac{2-x}{2}\right)G^0_{MgTi_2O_5} + x\left(\frac{x}{2}\right)G^0_{Al_3O_5^-} + x\left(\frac{2-x}{2}\right)G^0_{AlTi_2O_5^+} + (1-x)\left(\frac{x}{2}\right)G^0_{MgAl_2O_5^{2-}} - T\Delta S^{ideal} + G^E \quad (1)$$

The thermodynamic properties of all compounds listed in Table 1 (from Pelton et al [17] and the FactSage compound database [11]) are considered to be the most reliable estimates of the true data. In equation (2), $G^0_{MgTi_2O_5}$ for the real component is obtained from Table 1.

Table 1. Thermodynamic properties of the reviewed compounds

$$H\left(Jmol^{-1}\right) = A + \int_{298.15}^{T} C_P dT \qquad S\left(Jmol^{-1}K^{-1}\right) = B + \int_{298.15}^{T} \left(C_p / T\right)dT$$

$$C_p\left(Jmol^{-1}K^{-1}\right) = a + b(10^{-3})T + c(10^5)T^{-2} + dT^{-1/2} + e(10^8)T^{-3}$$

	A = Enthalpy	B= Entropy	a	b	c	d	e
TiO_2(s) (298-2130 K)	-944750	50.460	77.838		-33.678		4.0294
Ti_2O_3(β)[a] (470-2115 K)	-1519375	80.529	169.96		16.096	-750.22	-15.655
MgO(s) (298-3098 K)	-601500	26.951	61.110		-6.2115	-296.20	0.0584
Al_2O_3(s) (1200-2327 K)	-1656864	52.300	-787.52	0.06588	2638.2		0.0007
$MgTi_2O_5$(s) (298-1930 K)	-2504887	137.34	232.58		-56.608	-755.50	5.8214
Al_2TiO_5(s) (298-2500 K)	-2577174	128.45	249.29		-48.061	-1350.1	5.1603

The combination of the pseudocomponents is such that the solid solution is always electrically neutral. The pure Al_2TiO_5 compound is thus assumed to be an ideal equimolar mixture of $Al_3O_5^-$ and $AlTi_2O_5^+$, as is demonstrated by the following expression [16, 17]:

$$G^0_{Al_2TiO_5} = \frac{1}{2}\left(G^0_{Al_3O_5^-} + G^0{}_{AlTi_2O_5^+}\right) + 2RT\ln\left(\frac{1}{2}\right) \quad (2)$$

The value of $G^0_{Al_2TiO_5}$ is also obtained from Table 1. The Gibbs energies of the components and pseudocomponents of the solid solution are further related by the following exchange reaction:

$$\left(Mg^{2+}\right)_A\left(Ti^{4+}_2\right)_B O_5 + \left(Al^{3+}\right)_A\left(Al^{3+}_2\right)_B O_5^- = \left(Al^{3+}\right)_A\left(Ti^{4+}_2\right)_B O_5^+ + \left(Mg^{2+}\right)_A\left(Al^{3+}_2\right)_B O_5^{2-} \quad (3)$$

$$\Delta G_{MgTi_2O_5-Al_2TiO_5} = a' + b'T = G^0_{AlTi_2O_5^+} + G^0_{MgAl_2O_5^{2-}} - G^0_{MgTi_2O_5} - G^0_{Al_3O_5^-} \quad (4)$$

a' and b' are the adjustable empirical parameters of the model [16]. The standard Gibbs energy of one of the three pseudocomponents may be assigned an arbitrary value, followed by calculation of the other two from equations (2) and (4) and substitution into equation (1). The Gibbs energies of the four endmembers are then expressed in terms of the Gibbs energies of real components $MgTi_2O_5$ and Al_2TiO_5 [16, 17]. In equation (1), an additional excess Gibbs energy term, G^E, was included to account for solution non-ideality and is given as [17]:

$$G^E = c(1-x)(x)(2-x)/2 \quad (5)$$

where c is an empirical parameter. According to this expression, one binary interaction exists between Mg^{2+} and Al^{3+} on the A-sublattice when the B-sublattice is occupied by Ti^{4+}.
The thermodynamic model information generated here was incorporated into the FactSage software in order to produce a private $MgTi_2O_5$-Al_2TiO_5 solution database. To achieve this, the Gibbs energy expressions of the four respective endmembers and the G^E data were entered into the Gibbs energy minimization system (Compound Energy Formalism (CEF)) and the Redlich-Kister polynomial in FactSage to account for the ideal and the excess mixing respectively.

Methodology

The FactSage predictions were completed using the compositions and conditions that were used during the development of the current phase diagram. In this study, the PO_2 was varied between air or 0.21 atm (used by Jochens et al [10]) and 10^{-16} atm, a PO_2 deduced from the Ellingham diagram for the reduction of V_2O_3 to metallic V at a titanomagnetite smelting operational temperature of 1500°C (an estimate, as the operational PO_2 is of course not exclusively driven by the PO_2 for V metallization). The modelling was conducted using the FactSage customary search databases, i.e. pure solids database FactPS and oxides database FToxid, as well as the private $MgTi_2O_5$-Al_2TiO_5 solid solution database developed according to the above procedure. The phase equilibria and thermodynamic data relating to the titanomagnetite slags were plotted using the 'Phase Diagram' and 'Equilib' modules of the FactSage software.

The phase composition of a real plant titanomagnetite slag, viz. slag produced at Evraz Highveld Steel and Vanadium Corporation in South Africa (EHSV), was determined using Zeiss EVO® MA15 scanning electron microscope (SEM) coupled with a Bruker energy dispersive spectroscopy (EDS). The phase composition of the real slag was then evaluated against the phase equilibria in the current and proposed equilibrium phase diagrams.

Results and discussions

The current equilibrium phase diagram, as well as the FactSage predictions, was selected to cover a range of titanomagnetite slag compositions that are likely to be achieved with fluxing with limestone, dolomite or magnesite. As the first task of the current work, FactSage was used to reproduce the current phase diagram shown in Figure 1 [10]. The simulated phase equilibria (Figure 2) show that the liquidus temperature of the slags change from 1540°C at 30% CaO and 0% MgO to 1480°C at 0% CaO and 30% MgO, passing through a minimum of 1305°C at 20% CaO and 10% MgO. In terms of the liquidus surface, the current and simulated phase diagrams

are fairly comparable. In terms of the phase equilibria, it appears that at high CaO levels there is agreement that $CaO.TiO_2$ is the primary phase. However there is a difference at higher MgO levels in that the FactSage simulation suggests that the primary phase is generally a titania spinel, a solid solution of $(Mg)(Al,Ti)_2O_4$ and ($MgAl_2O_4$-$MgTi_2O_4$), followed by Mg_2SiO_4 (or $MgTi_2O_5$-Al_2TiO_5 at 3%CaO and 27%MgO and above), with $MgTi_2O_5$-Al_2TiO_5 forming as a ternary phase. This is in contrast with the current phase diagram, which shows that the primary phase is a pseudobrookite-type solid solution with stoichiometry $4MgTi_2O_5$-Al_2TiO_5. Thus, with dolomite flux alone, $4MgTi_2O_5$-Al_2TiO_5 crystallizes as a primary phase, followed by forsterite (Mg_2SiO_4) with no prediction of the formation of the spinel. For the purpose of studying the effect of PO_2 on the titanomagnetite slag liquidus surface and phase equilibria, the simulated phase diagram was accepted as a true reflection of phase equilibria of fluxed titanomagnetite slags in air.

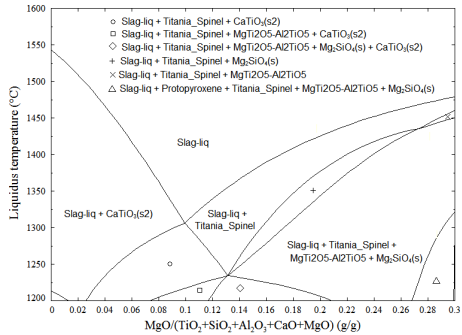

Figure 2: Simulated equilibrium phase diagram at PO_2 = 0.21 atm for the slag system: TiO_2 = 37.19%, SiO_2 = 19.69%, and Al_2O_3 = 13.12, at varying proportions of CaO (30-%0) and MgO (0-30%)

Effect of PO_2 on liquidus surface and phase equilibria

The effect of PO_2 on the liquidus surface of titanomagnetite slags was studied across the compositional range investigated by Jochens et al [10]. Figure 3 shows the liquidus temperatures plotted as a function of CaO/MgO ratio, i.e. MgO where CaO = 30-MgO, under varying PO_2 concentrations. It appears that the liquidus surface in the TiO_2-SiO_2-Al_2O_3-MgO-CaO system with a composition comparable to a fluxed titanomagnetite slag increases with decreasing the PO_2. This observation concurs with the findings of Nityanand et al [18] who studied the effect of TiO_2 additions and PO_2 on liquidus temperatures of some CaO-Al_2O_3 melts, and found that at low PO_2 and high TiO_2 contents there is a continuous increase of the liquidus temperatures.

The effect of PO_2 was investigated further on the dolomite-fluxed titanomagnetite slag composition, which falls in the spinel primary phase field and is currently operated by EHSV. Figure 4 shows the changes of liquidus temperatures as a function of PO_2 at fixed composition of the slag. It appears that the spinel generally crystalizes as a primary phase, except at PO_2 of between 10^{-10} and 10^{-15} atm where the primary phase is a pseudobrookite solution.

Oxidized titanium species, i.e. Ti^{4+}, are readily reduced to lower-oxidation-state titanium species when subjected to high temperature reducing conditions applicable to ironmaking processes [9]. The reduction of the Ti^{4+} has the potential of affecting the phase equilibria. In the present work, the effect of PO_2 on the phase equilibria was simulated by monitoring the reduction of titanium species. Figure 5 shows the Ti^{3+}/ Ti^{4+} mass fraction ratio, i.e. the measure of the reduction of Ti species in the molten slag, plotted as a function of PO_2 in the range of 0.21 atm to 10^{-16} atm. The results predict an increase in Ti^{3+}/ Ti^{4+} mass fraction ratio with decreasing PO_2. This implies that by decreasing PO_2 to the range applicable in titanomagnetite smelting, the phase equilibria of the slag will diverge from the phase equilibria developed by Jochens et al [10].

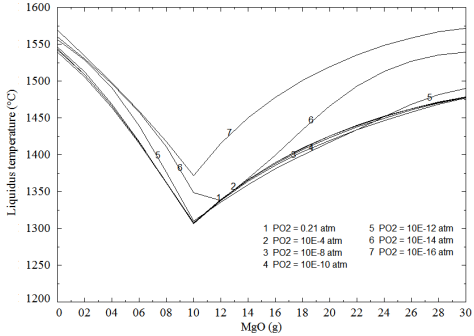

Figure 3: Effect of PO_2 on the liquidus surface of the titanomagnetite slag of the composition: TiO_2 = 37.19 g, SiO_2 = 19.69 g and Al_2O_3 = 13.12 g, with varying proportions of CaO (30-0 g) and MgO (0-30 g)

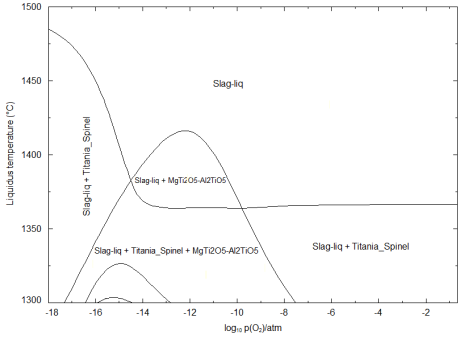

Figure 4: Effect of PO_2 on the liquidus surface and phase equilibria of the (dolomite) fluxed titanomagnetite slag with the composition: TiO_2 = 37.19 g, SiO_2 = 19.69%, and Al_2O_3 = 13.12%, MgO = 14% and CaO = 16%

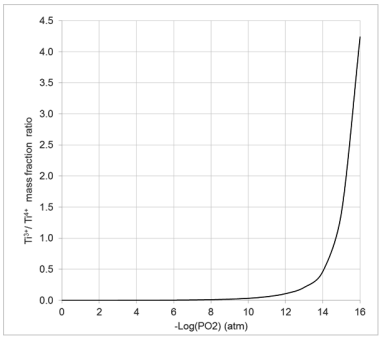

Figure 5: Effect of PO_2 on the titanium reduction in the fluxed titanomagnetite slag with the composition: TiO_2 = 37.19 g, SiO_2 = 19.69%, and Al_2O_3 = 13.12%, MgO = 14% and CaO = 16%

Proposed equilibrium phase diagram for titanomagnetite slags

Figure 6 is proposed as a revised intermediate equilibrium phase diagram for predicting phase compositions of fluxed titanomagnetite slags that conform to a typical composition: 37.19% TiO_2, 19.69% SiO_2, 13.12% Al_2O_3, and 30.00% of various ratios of CaO+MgO. The proposed equilibrium phase diagram shows that the liquidus surface of titanomagnetite slags varies around an average liquidus temperature of 1570°C in the composition range of 30% CaO and 0% MgO to 0% CaO and 30% MgO, passing through a minimum of 1370°C at 20% CaO and 10% MgO. It appears that at high CaO levels, the primary phase to crystallize is perovskite ($CaO.TiO_2$), whereas at high MgO levels, the primary phase is a spinel solid solution, i.e. $(Mg)(Al,Ti)O_4$. The proposed equilibrium phase diagram does not show the possible competition between primary phases, i.e. $(Mg)(Al, Ti)O_4$ and $MgTi_2O_5$-Al_2TiO_5, that was observed previously. Modelling with Ti_3O_5 as a component of $MgTi_2O_5$-Al_2TiO_5 together with experimentation are required to verify and update the proposed liquidus surface and phase equilibria.

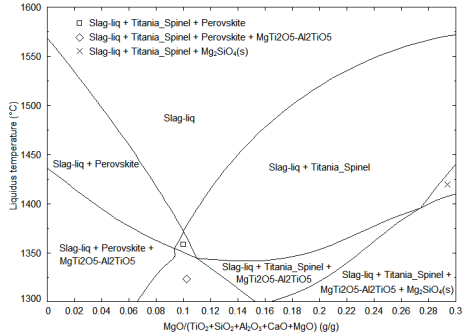

Figure 6: Proposed intermediate equilibrium phase diagram developed at PO_2 of 10^{-16} atm for the fluxed titanomagnetite slags that conform to the reviewed composition

Phase composition of a real plant titanomagnetite slag

The phase composition data of a real plant titanomagnetite slag using the dolomite-fluxed slag produced by EHSV as a case study were required to examine the ability of the proposed phase diagram to predict the phase compositions of fluxed titanomagnetite slags. The phase composition results of the EHSV titanomagnetite slag are shown in Figure 7. The intensities and shapes of the crystals of pseudobrookite ($MgTi_2O_5$-Al_2TiO_5) and spinel [$(Mg)(Al,Ti)O_4$] phases in the real EHSV slag suggest that any of the two phases could have crystallized first directly from liquid phase. From this data, it is still not clear which of the two phases is a primary phase.

The real EHSV titanomagnetite slag is produced under reducing conditions, which are essential for vanadium metallization. According to Ellingham diagrams, the vanadium metallization PO_2 of about 10^{-16} atm at 1500°C is near to the transition for crystallization of the $(Mg)(Al,Ti)O_4$ and $MgTi_2O_5$-Al_2TiO_5 primary phases as shown in Figure 4. The EHSV phase composition concurs with the proposed phase diagram in Figure 6 in terms of spinel primary crystallization; however, the phase diagram does not predict the possibility of $MgTi_2O_5$-Al_2TiO_5 crystallizing first.

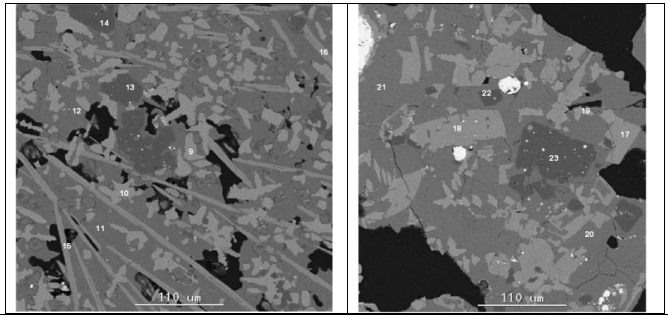

	MgO	Al_2O_3	SiO_2	CaO	TiO_2	V_2O_5	FeO	Total	Phases
9	0.2	0.4	0.0	39.7	55.3	0.3	0.0	95.9	Perovskite
10	0.1	0.2	0.1	39.6	55.8	0.1	0.0	95.9	Perovskite
11	18.0	11.3	30.5	18.5	15.3	0.3	0.3	94.2	Non-crystalline
12	13.9	8.2	38.7	22.1	12.6	0.1	0.2	95.8	Non-crystalline
13	28.9	60.6	0.1	0.0	11.3	1.7	0.3	102.9	Spinel
14	28.9	63.0	0.2	0.1	8.0	2.3	0.2	102.7	Spinel
15	9.4	2.0	0.7	1.0	81.6	0.3	0.6	95.6	Pseudobrookite
16	8.9	2.1	0.3	0.7	82.3	1.1	0.2	95.6	Pseudobrookite
17	5.8	2.7	0.1	0.2	90.3	0.2	0.1	99.4	Pseudobrookite
18	9.3	1.8	0.3	0.3	86.6	1.9	0.0	100.2	Pseudobrookite
19	0.2	0.3	0.1	39.5	56.1	0.0	0.1	96.3	Perovskite
20	10.5	9.7	34.8	23.4	16.7	0.1	0.2	95.4	Non-crystalline
21	9.6	10.1	34.3	23.9	18.6	0.4	0.2	97.1	Non-crystalline
22	28.1	65.2	0.3	0.1	7.9	0.7	0.4	102.7	Spinel
23	27.6	62.5	0.5	0.2	9.2	1.4	0.4	101.8	Spinel

Figure 7: Typical backscattered electron images and EDS analysis results (mass%) of a titanomagnetite slag produced by EHSV

Conclusions

The following conclusions can be made:

- Liquidus temperature and Ti^{3+}/ Ti^{4+} mass fraction ratio, i.e. the reduction of Ti species, of compositionally-matching titanomagnetite slags both increase with decreasing PO_2
- At higher MgO concentrations, the spinel generally crystallizes as the primary phase, whereas at PO_2 of between about 10^{-10} and 10^{-15} atm the primary phase may be a pseudobrookite-type solution.
- The proposed intermediate equilibrium phase diagram of titanomagnetite slags with the applicable chemical compositions is as shown in Figure 6.
- When dolomite-fluxed smelting is conducted at PO_2 of about 10^{-16} atm, the primary phase is either a spinel or a pseudobrookite. This scenario was observed experimentally in the phase composition of the titanomagnetite slag produced by EHSV.

More complex modelling with $MgTi_2O_5$, Al_2TiO_5 and Ti_3O_5 endmembers together with experimental measurements are underway to verify and update the intermediate phase diagram generated in the present work. The liquidus surface and phase equilibria at various TiO_2 grades should be investigated further to cover a wide range of titanomagnetite resources.

Acknowledgment

The authors wish to thank the following for their inputs: A.D. Pelton, M.W. Erwee and A. Corfield. Financial support of Mintek is greatly appreciated.

References

1. L. Zhang, L.N. Zhang, M.Y. Wang, T.P. Lou, Z.T. Sui, and J.S. Jang, "Effect of perovskite phase precipitation on viscosity of Ti-bearing blast furnace slag under the dynamic oxidation condition", *Journal of crystalline solids*, 352 (2006), 123-129.
2. B.F. Kelly, "Ironmaking at BHP New Zealand Steel Limited, Glenbrook, New Zealand", *Australasian Mining and Metallurgy, The Sir Maurice Mawby Memorial Volume*, 1 (1993), 348-353.
3. W.S. Steinberg, W. Geyser, and J. Nell, "The history and development of the pyrometallurgical processes at Evraz Highveld Steel and Vanadium", *Southern African Institute of Mining and Metallurgy* (2011), 63-76.
4. D.S. Van Vuuren, and G.T. Tshilombo, "Nitriding of ilmenite and high-grade slag fines", *Journal of the South African Institute of Mining and Metallurgy* (2011), 173-181.
5. J.H. Becker, "Recovery of titanium from titanium bearing materials". *United States Patent 7258847*, (2002), (Accessed on 2015-10-26).
6. O.A. Fouad, "Upgrading of a low – grade titanium slag by sulphation roasting technique to produce synthetic rutile", *Acta Metallurgical Slovaca, 11(1)* (2005), 14-24.
7. L. Zhang, L.N. Zhang, M.Y. Wang, G.Q. Li, and Z.T. Sui, "Recovery of titanium compounds from molten Ti-bearing blast furnace slag under the dynamic oxidation condition", *Minerals Engineering*, 20 (2007), 684-693.

8. P.C. Pistorius, "Titania slag smelting and calcination of crude zinc oxide: examples of processing under thermodynamic and kinetic constraints", *Proceedings of the second international slag valorization symposium, Leuven Belgium,* (2011), 263-270.
9. B. Zhao, E. Jak, and P. Hayes "Phase equilibria studies in the slag system TiO_2-SiO_2-Al_2O_3-MgO-CaO at carbon saturation", *Eighth International Conference on Molten Slags, Fluxes and Salts, Santiago, Chile,* (2009), 71-82.
10. P.R. Jochens, G. Sommer, and D.D. Howat, "Preliminary equilibrium and non-equilibrium phase studies of titaniferous slags", *Journal of The iron and Steel Institute,* 207 (1969) 187-192.
11. C.W. Bale, P. Chartrand, S.A. Degterov, G. Eriksson, K. Hack, R. Ben Mahfoud, J. Melancon, A.D. Pelton, and S. Petersen, "FactSage thermochemical software and databases", Chalphad, 25 (2) (2002), 189-228.
12. V. Buscaglia, G. Battilana, and M. Leoni, "Decomposition of Al_2TiO_5-$MgTi_2O_5$ solid solutions: a thermodynamic approach", *Journal of materials science,* 31 (1996), 5009-5016.
13. D. Xirouchakis, A. Smirnov, K. Woody, D.H. Lindsley, and D.J. Andersen, "Thermodynamics and stability of pseudobrookite-type $MgTi_2O_5$ (karrooite)", *American mineralogist,* 87 (2002), 658-667.
14. A. Navrotsky "Thermodynamics of formation of some compounds with pseudobrookite structure and of the $FeTi_3O_5$-Ti_3O_5 solid solution series", *American mineralogist,* 60 (1975), 249-256.
15. T. Epicier, G. Thomas, H. Wohlfromm, and J.S. Moya, "High resolution electron microscopy study of the cationic disorder in Al_2TiO_5", *Journal of material research, 6 (1)* (1991), 138-145.
16. G. Eriksson, A.D. Pelton, E. Woermann, and A. Ender, "Measurement and thermodynamic evaluation of phase equilibria in the Fe-Ti-O system", *Physical chemistry,* 100 (11) (1996), 1839-1849.
17. A.D. Pelton, G. Eriksson, D. Krajewski, M. Gobbels, and E. Woermann "Measurement and thermodynamic evaluation of phase equilibria in the Mg-Ti-O system", *Zeitschrift fur physikaliche chemie,* 207 (1998), 163-180.
18. H. Nityanand, and H.A. Fine "The effect of TiO_2 additions and oxygen potential on liquidus temperatures of some Ca-Al_2O_3 melts", *Metallurgical and Materials Transactions B,* 14 (4) (1983) 685-692.